Ultrafast all-optical switching

Zeev Zalevsky, David Mendlovic, Emanuel Marom, Nadav Cohen, Efraim Goldenberg, Naim Konforti, Amir Shemer, Gal Shabtay, Uriel Levy, and Roy Appelman

Civcom Devices and Systems Incorporated, Petach-Tikva 49514, Israel
zeev.z@civcom.com

Received 27 February 2002; revised manuscript received 19 April 2002

We present innovative concepts related to the realization of ultrafast optical switches to be used for obtaining all-optical switching. We review the construction and the achievements of Civcom Incorporated during its research and development stages of constructing its ultrafast switch. Experimental measurements are exhibited. © 2002 Optical Society of America

OCIS codes: 060.0060, 060.1810, 060.2330, 060.2340.

1. Introduction

Over the past few years significant changes in optical networking have occurred. Ever increasing demand for data services have been the driving force behind the wide deployment of dense wavelength-division-multiplexing (DWDM) technologies to increase network capacity. These networks were designed to provide the maximum bandwidth possible while not incorporating true optical-layer functionality. Today the force behind the deployment of new intelligent optical networks is service providers' need to decrease operational costs and increase revenues by providing services based on a new breed of optical components. These components are characterized by new optical functionality and by multiple function integration. One such component is the optical switch. The switch has evolved from a simple optomechanical device to an integrated component operating at higher speeds and incorporating new functions. The addition of new capabilities, such as dynamic variable optical attenuation (VOA) and optical multicast, into the optical switch component, together with the increase in operation speed, offers significant advantages and enables a variety of new applications.

The establishment of synchronous optical network and synchronous digital hierarchy (SONET/SDH) as the dominant transport technology has introduced some de facto standards into network-protection schemes. The emerging practice has tended toward use of dual homing (or no protection) in the network access, self-healing SONET/SDH rings in the metropolitan area network (MAN), and 1:1 or 1:*N* (primarily) linear protection in the long haul.[1] The evolution toward intelligent optical networks has led to the need for new, all-optical protection schemes to address a wide variety of network architectures, such as rings, linked rings, hybrid mesh–ring and mesh architectures. The integration of switching, multicast, and attenuation control is extremely useful in designing such protection schemes. For example, some of the best-known ring-protection schemes are DPRING (dedicated protection ring) and the OMS-SPRING (optically multiplexed section sheared protection ring) protection architectures (Fig. 1).

This paper reviews the research and development stages of Civcom Incorporated in its construction of the all-optical ultrafast switch. This switch is capable of multicast functionality as well as VOA operation. The preliminary design was based on multistage interconnection networks with a polarization-sensitive approach. Eventually, a wavelength- and polarization-insensitive switch for obtaining strictly nonblocking connectivity was achieved. Section 2 discusses the concept of the multistage interconnection network. A preliminary prototype is presented in Section 3. Improved engineering design is shown in Section 4.

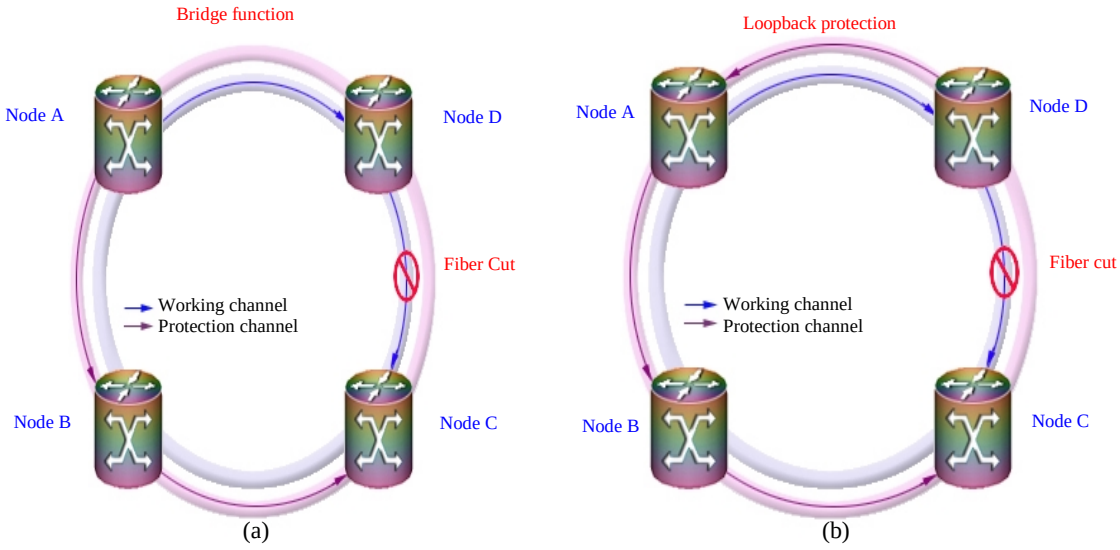

Fig. 1. (a) DPRING protection scheme, (b) OMS-SPRING protection scheme.

Section 5 presents the environmental test procedure applied over the improved prototype. The paper is concluded in Section 6.

2. Multistage Interconnection Networks

The switch architecture that was initially used was described by Mendlovic *et al.*[2,3] Their polarization-coded inputs are dynamically controlled by electrically addressed retarders. That switch constructed in a multistage interconnection network (MIN) is based on a building block, which was a 2×2 switch. The switching element is based on a controlled $\lambda/2$ plate placed in between two birefringent calcite crystals that act as beam displacement plates (BDPs). This approach has been demonstrated for 2×2 and for 4×4 optical switches.[3,4] The basic structure of this switch is shown in Fig. 2.

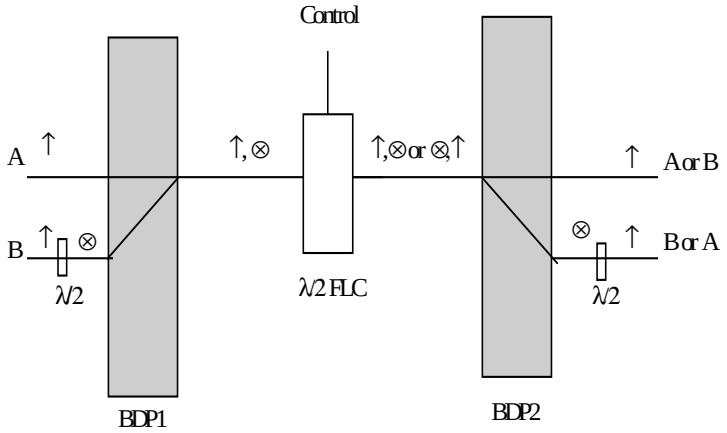

Fig. 2. 2×2 bypass exchange switch based on polarization coding with birefringent calcite crystals as BDPs and FLC $\lambda/2$ retarder switch.

In this system the two incoming signals A and B are linearly polarized and combined, for example, by use of a $\lambda/2$ plate in the entrance plane of signal B followed by the calcite BDP1. The resultant ray then passes through a controlled $\lambda/2$ ferroelectric liquid-crystal

(FLC) pixel and is reopened by the second calcite BDP2. When a proper voltage is applied to the FLC pixel, it acts as a λ/2 pixel and the polarization of the signals A and B interchange, thus obtaining an exchanged state of the inputs in the output plane. With no voltage applied, the FLC is transparent to the incoming signals and the output is identical to the input (bypass mode). The final λ/2 plate in the output plane restores the output polarization of the second beam. A similar approach is used to achieve the 2 × 2 broadcast switch (Fig. 3).

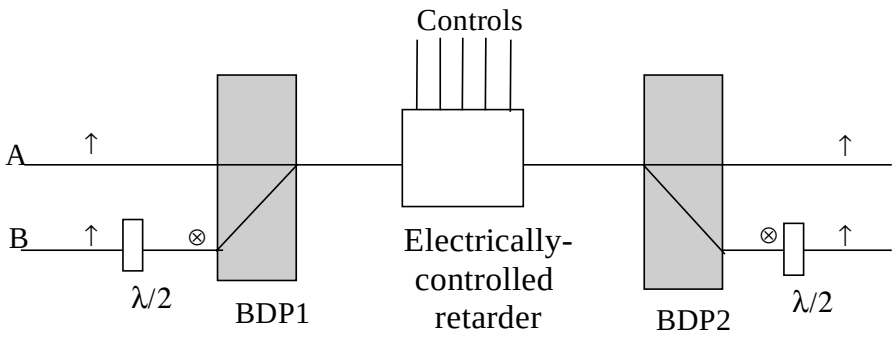

Fig. 3. Proposed setup for the 2 × 2 broadcast switch.

By replacing the controlled λ/2 FLC pixel in between the two calcites with a more sophisticated retarder that allows the retardation level to be controlled in fine steps, we obtain the four possible states of the broadcast switch and may achieve even greater flexibility. For instance, the λ/2 FLC block may be replaced with two pixels of λ/4 FLC.

The bypass and exchange modes are obtained by means of activating the retarder to 0- or 90-deg retardation, respectively. The two broadcasting modes are achieved by means of activating the retarder to retardation of 45 deg and blocking one of the inputs (signal B for the upper broadcast mode and signal A for the lower broadcast mode).

By limiting the system to use of these four modes, we achieve an important property of this switching system: the division of the broadcasted input signal into two energy-equivalent output signals. Thus, in MIN systems consisting of several 2 × 2 broadcast switches, we can activate the broadcast state in the proper switches to divide the energy of the input signal evenly among the connected outputs (for an even pair of outputs).

It is not necessary, though, to impose those limitations. In the more general case, both inputs are always connected to the switch, and the retardation level is arbitrary. In this way, the generalized 2 × 2 system depicted in Fig. 4 is achieved. With that setup both input signals are divided into two parts, X and Y. The X part of one signal is added to the Y part of the other. X and Y are dependant and reflect the retardation level. If one wishes to set X and Y to independent levels, an additional attenuator should be used on one of the signals. Note that the signals A and B represent the input intensity.

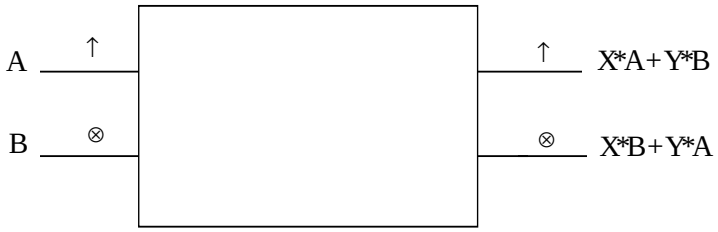

Fig. 4. Generalized 2 × 2 broadcast and switching system.

3. Prototype and Experimental Results

A demonstrator based on the design guideline stated in Section 2 was constructed. The light source used is a doubled Nd:Yag laser (530-nm wavelength). An input mask was placed at the input plane. The constructed switch is a 16×16 switch consisting of 2×2 modules. The device is depicted in Fig. 5 where the optical core itself occupies a volume of less than 3 cm^3. The state of each FLC controls the operation of the switch bypass, exchange, or broadcast. The panels are driven by dedicated hardware, which is computer controlled.

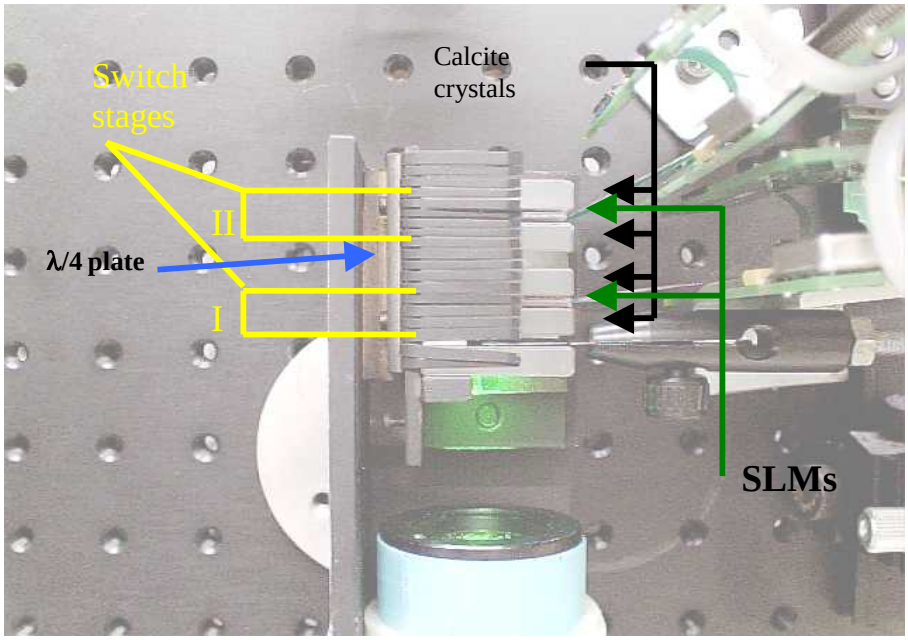

Fig. 5. All-optical 16 ×16 switch. SLM, spatial light modulator.

Special software was written to control the state of each FLC. By controlling all the FLCs, and changing their status in a synchronous manner, we can achieve the entire range of possible output patterns.

Figure 6 shows some of the captured results that demonstrate a few of this system's operational modes (switching, bypassing, and broadcasting).

The main disadvantage of the suggested configuration is that the dynamic elements used to perform the switching operation were FLCs, which are not ultrafast (they allow switching speeds of 100–500 μs). In addition, to obtain larger switches, an omega 2 MIN network was used. This network cannot allow a strictly nonblocking connectivity between the input and the output channels. To overcome this, Civcom's solutions are currently based on a different type of dynamic electro-optic materials. As seen in Fig. 6, the first prototype did not manage to achieve adequate cross talk between output optical channels.

4. Improved Design Progress

The improved design included a change of the optical configuration as well as the electro-optical material. A faster material was used as the dynamic element. The material was mapped and integrated into a unique configuration allowing strictly nonblocking

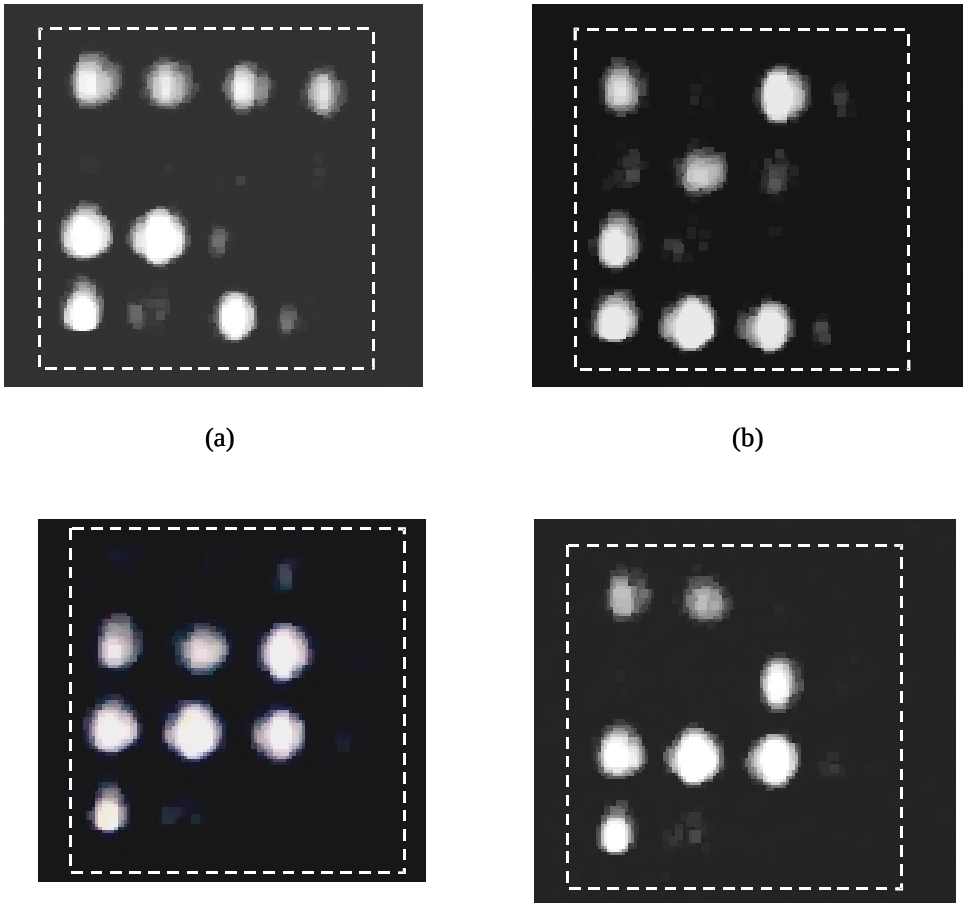

Fig. 6. Some experimental results of different interconnection configurations.

connectivity, and the designed prototype was wavelength and polarization insensitive.

The experiment shown in Fig. 7 presents the polarization rotation ability of the new material. The figure depicts the first $\pi/2$ behavior of the material as a function of normalized voltage. As can be seen from the graph, the material has a linear behavior between the square of the operating voltage and the rotation of the polarization angle. This linearity starts from a certain voltage and greater. This behavior might be explained when we consider that the material exhibits a basic (natural) birefringence that exists when no voltage is applied to the device.

The true relation between the rotation of the polarization angle α and the applied voltage V corresponds to the electro-optic effect (Kerr effect) as expressed in Eq. (1):

$$\alpha = \frac{\pi V^2}{2V_\pi (\lambda)^2}, \tag{1}$$

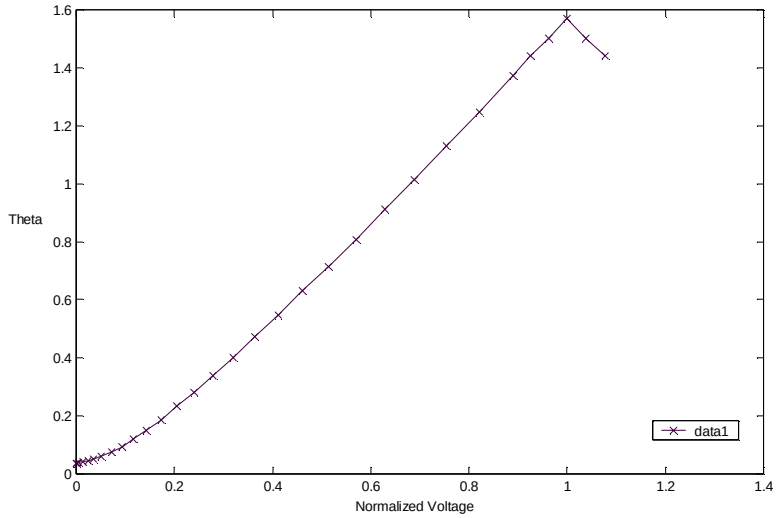

Fig. 7. Rotation of polarization angle (α) versus the square of the voltage.

where λ is the illuminating wavelength, V is the applied voltage, and $V_\pi(\lambda)$ is the voltage (which is wavelength dependent) required for rotating the polarization angle in angle of π. This effect itself results from the imposed electric field that causes the asymmetric molecules of the material to align with the field. This causes the material to become anisotropic and birefringent. The change in the refraction index is given by

$$n_o - n_e = \lambda K \frac{V^2}{d^2}, \tag{2}$$

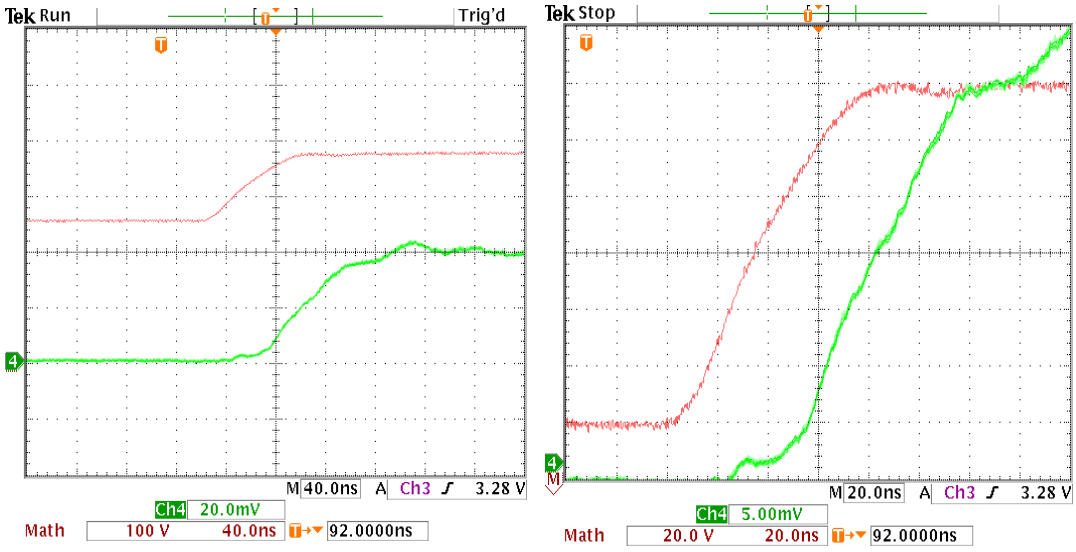

(a) (b)

Fig. 8. Rise time results as measured with a fast discharge circuit. (a) For 40-ns time division, (b) for 20-ns time division.

where n_o and n_e are the ordinary and the extraordinary refraction indices, K is the Kerr constant (which is dependent upon the wavelength), V is the applied voltage, d is the distance between the electrodes, and λ is the wavelength. This dynamic material exhibits loss of less than 4% and an extinction ratio of more than 1:800.

The above-mentioned electro-optic material is tolerant to high-power signals, and a valid operation was measured for an input signal with a power of 5 W.

Figure 8 presents the material's performance. The best device had a discharge time of 100 ns. The prototype constructed for performing the described measurements is extremely small in dimensions as can be seen in Fig. 9.

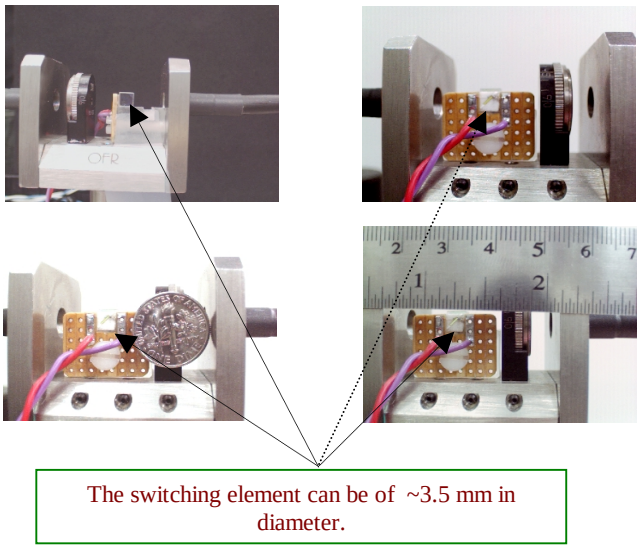

Fig. 9. Switching prototype.

In addition to the operating rate mapping, various additional experiments were performed. For instance, for exploring the thermal dependence. The polarizers were in a cross state, and $V_{3\pi}$, $V_{2\pi}$, V_{π} were measured between 25 and 100 °C. Note that V_{α} denotes the normalized voltage required for obtaining an α rotation of the polarization angle with respect to V_{α} at 25 °C. The measurement was of the actual optical power impinging at the optical detector. No modulation was applied, and only dc voltages were used. Figure 10 presents the obtained results where the *y*-axis values were normalized to the voltage that was required at 25 °C.

The thermal dependence presented in Fig. 10 might be eliminated with a thermal control based on a thermoelectric cooler or a heater.

Subsequently, an improved prototype was constructed (see Fig. 12 below). Its optical configuration, which incorporates the dynamical electro-optical element together with BDP, revealed an optical cross talk between adjacent channels of below −45 db. Figure 11 provides a visual display of the obtained cross-talk measurements. Figure 11(a) presents the switching when the light is directed toward the upper output channel while no light is seen in the lower output channel (low cross talk). In Fig. 11(b) the switching directs the light to the lower output channel while no light is seen in the upper channel. In 11(c) the multicast functionality is displayed, and the light is simultaneously directed to both output channels. The results were obtained for a wavelength of 1550 nm.

The optical switch used to perform the cross-talk measurements is demonstrated in Fig. 12. A special electrical driver was developed in order to induce the optical response and to eliminate its various temporal fluctuations.

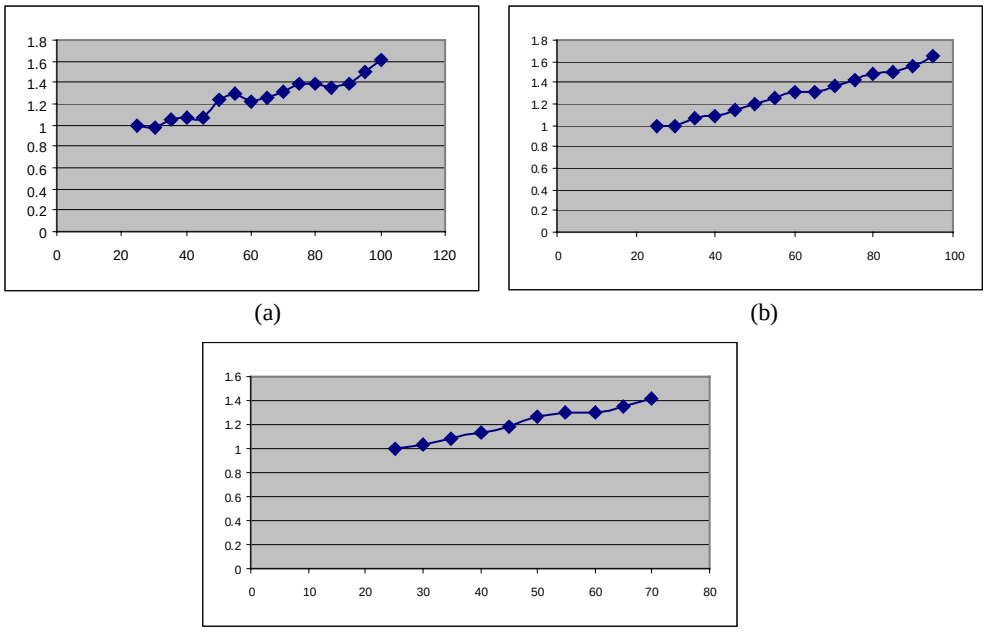

Fig. 10. Thermal dependence of the operation voltage for (a) V_{π}, (b) $V_{2\pi}$, and (c) $V_{3\pi}$.

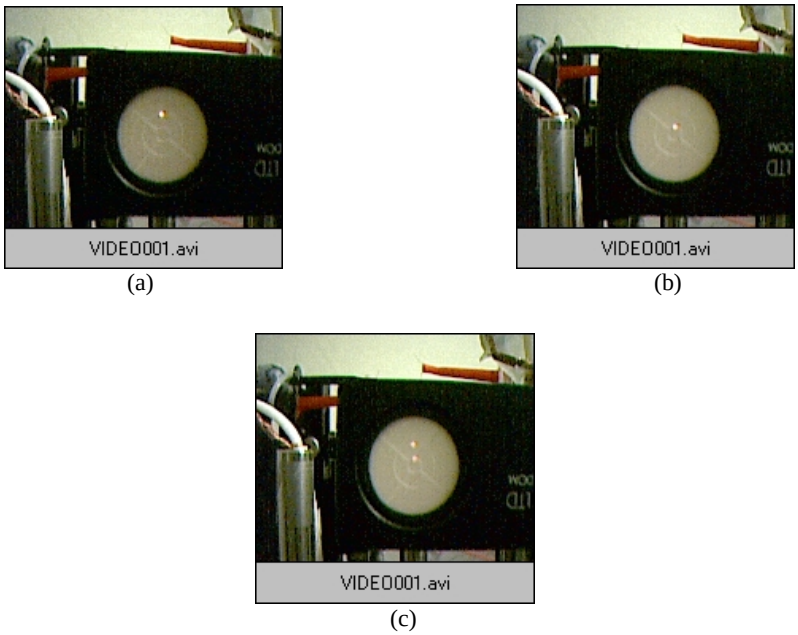

Fig. 11. Cross-talk demonstration in the 1×2 all-optical improved prototype.

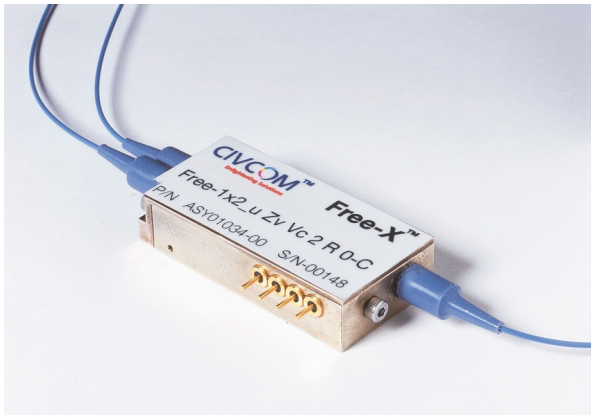

Fig. 12. Civcom's improved 1 × 2 switching prototype.

Figure 13 presents the switching time obtained during operation of a complete switch. The figure presents the rise time and the fall time of the optical response. The scope computed the 10–90% response time. For the electrical driver parameters chosen for this figure the overall optical response time as measured by the scope was approximately 250 ns (seen in the right-hand part of the figure).

The optical performance of the improved 1 × 2 switching prototype of Fig. 12 as measured in a certified optical laboratory are presented in Fig. 14, which shows the measured insertion losses, cross talk, and polarization-dependent losses (PDLs) as a function of the wavelength over the spectral C band. The polarization-mode dispersion (PMD) of output channel number 1 is depicted in Fig. 14(d).

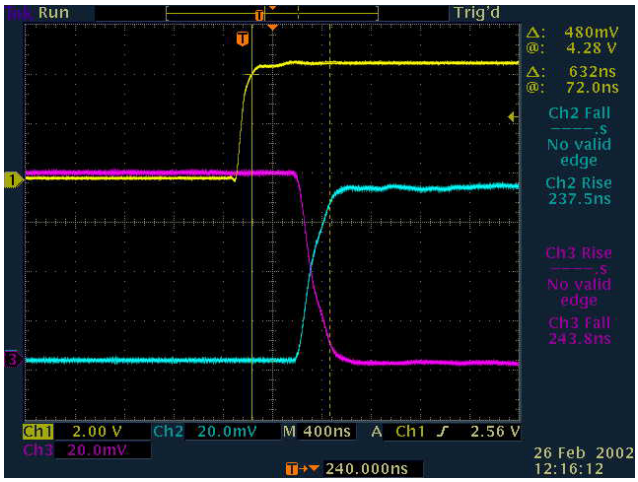

Fig. 13. Development of special electrical driver providing induced optical response with rise time and fall time of 250 ns.

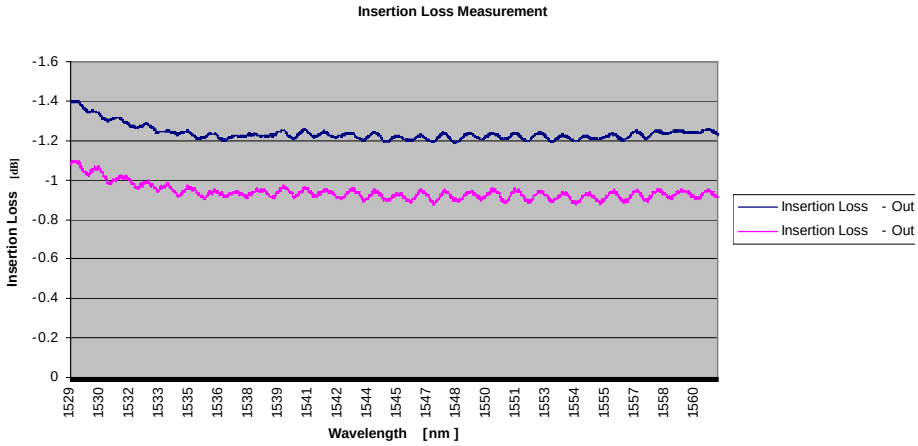
Insertion Loss Measurement
Insertion Loss [dB]
-1.6
-1.4
-1.2
-1
-0.8
-0.6
-0.4
-0.2
0
1529 1530 1532 1533 1535 1536 1538 1539 1541 1542 1544 1545 1547 1548 1550 1551 1553 1554 1555 1557 1558 1560
Wavelength [nm]
Insertion Loss - Out
Insertion Loss - Out

(a)

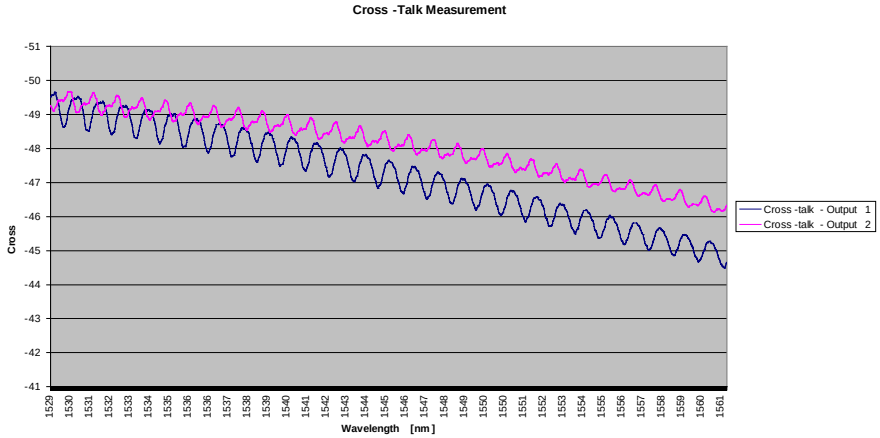
Cross -Talk Measurement
Cross
-51
-50
-49
-48
-47
-46
-45
-44
-43
-42
-41
1529 1530 1531 1532 1533 1534 1535 1536 1536 1537 1538 1539 1540 1541 1542 1543 1544 1545 1546 1547 1548 1549 1550 1550 1551 1552 1553 1554 1555 1556 1557 1558 1559 1560 1561
Wavelength [nm]
Cross -talk - Output 1
Cross -talk - Output 2

(b)

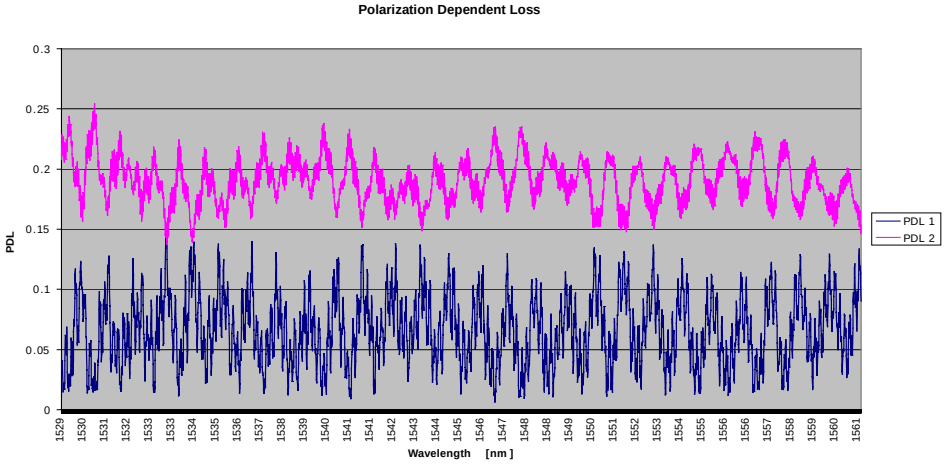
Polarization Dependent Loss
PDL
0.3
0.25
0.2
0.15
0.1
0.05
0
1529 1530 1531 1532 1533 1533 1534 1535 1536 1537 1538 1539 1540 1541 1541 1542 1543 1544 1545 1546 1547 1548 1548 1549 1550 1551 1552 1553 1554 1555 1556 1556 1557 1558 1559 1560 1561
Wavelength [nm]
PDL 1
PDL 2

(c)

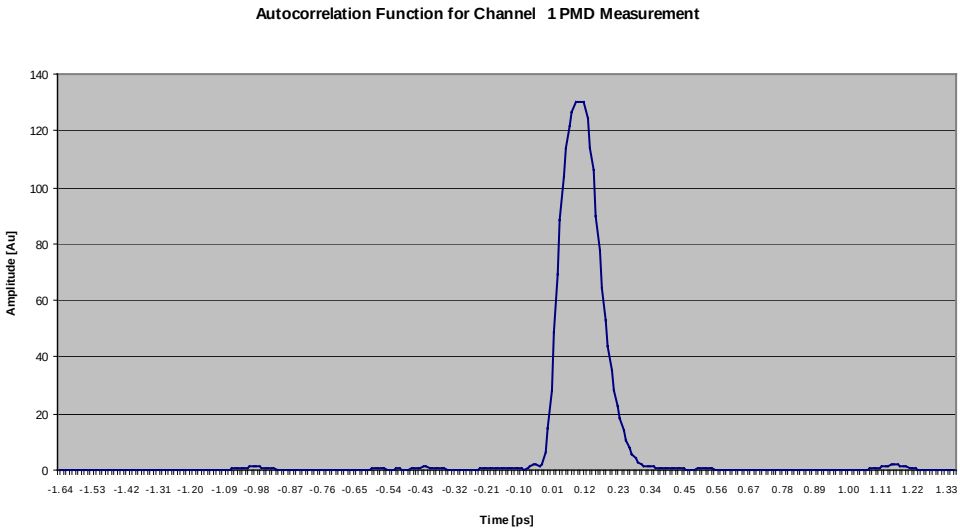

(d)

Fig. 14. Optical performance of the improved 1×2 switching prototype: (a) Insertion loss, (b) cross talk, (c) PDL, (d) PMD.

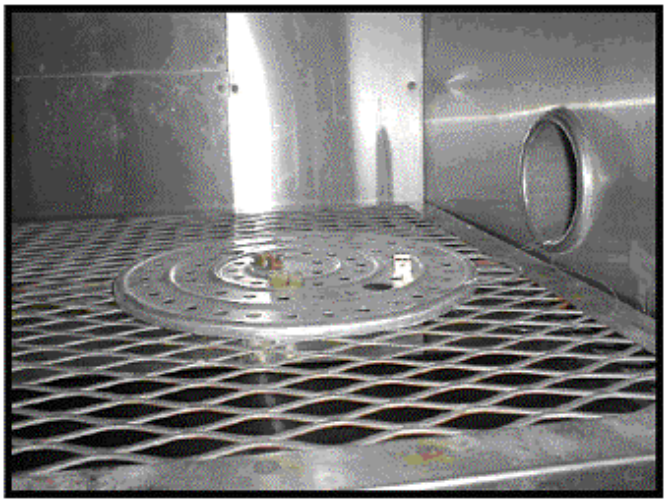

Fig. 15. Temperature cycling chamber testing.

5. Environmental Testing

Civcom's prototype switch successfully passed preliminary environmental testing as specified by GR 1221 (GR, general requirements). In the testing, not only was the switch itself not physically damaged; its optical performance was not affected. Figure 15 presents the optical submodules connected to a special jig placed in a temperature cycling chamber.

Figure 16 displays the temperature cycling chart.

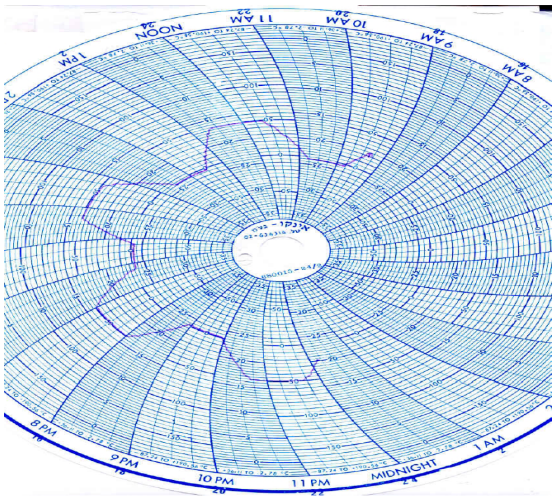

Fig. 16. Temperature cycling chart.

In Fig. 17(a) the switch is mounted on an electrodynamic shaker. The sine vibration test graph is seen in Fig. 17(b). Figure 18 presents the switch mounted on the shock machine.

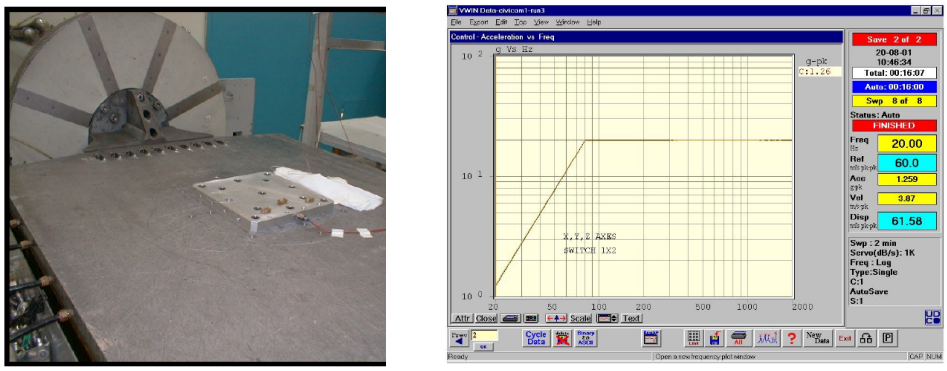

(a) (b)

Fig. 17. Electrodynamics shaker.

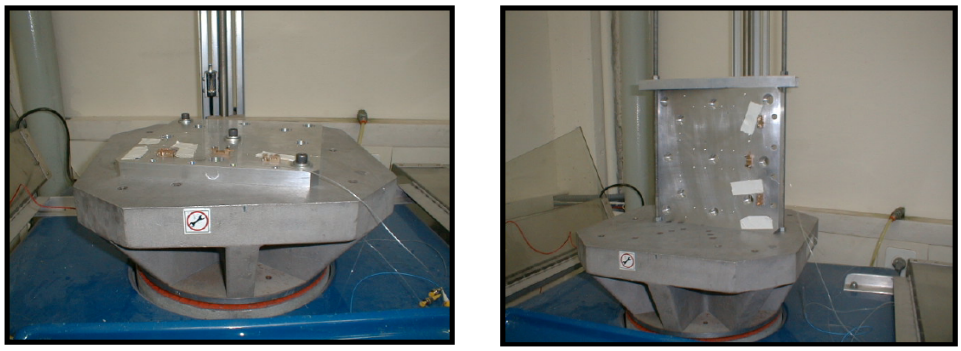

(a) (b)

Fig. 18. Switch mounted on the shock machine.

The mechanical shock test graph is seen in Fig. 19. Table 1 presents a measured datasheet of Civcom's present technical performance for 1×2 and 2×2 switches, as discussed in this paper.

6. Conclusions

This paper has reviewed the research and development stage of Civcom Incorporated in which, it is believed, the first ultrafast all-optical switch was developed. Experimental results of the designed prototype were demonstrated. Further improvements are to be obtained at Civcom in the near future.

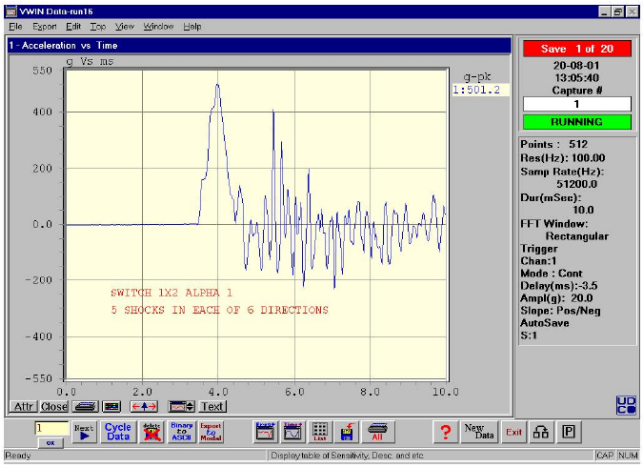

Fig. 19. Mechanical shock test graph.

Table 1. Technical Specifications of Civcom's Switch

Parameter	Unit	1 × 2 Fast Switch Specification	2 × 2 Fast Switch Specification
Wavelength window	nm	1525–1625	1525-1625
Insertion loss	dB	1.4 ± 0.2	1.6 ± 0.2
Back reflection	dB	Max –50	Max –50
Cross talk	dB	–45	–45
PDL	dB	0.2	0.2
Switching time	ns	250	250
Optical input power	dBm	Typical 25, max 36	Typical 25, max 36
Operating temperature	°C	–10 to +60	–10 to +60
Dimensions (optical module)	mm	54 (L) × 35 (W) × 14 (H)	62 (L) × 36 (W) × 15.5 (H)
Reliability	cycles	$>10 \times 10^9$	$>10 \times 10^9$
VOA dynamic range	dB	20	20
VOA granularity	dB	0.2	0.2
Input voltage	V_{dc}	12	12
Switching frequency	kHz	20	20
Weighted multicast (and broadcast) granularity	%	5 (higher granularity available)	5 (higher granularity available)
PMD	ps	0.1	0.1

References

1. S. Ayandeh and P. Veitch, "Dynamic protection and restoration in multilayer networks" (Optical Internetworking Forum, Paris, France, 2001), p. 166, http://www.oiforum.com.
2. D. Mendlovic, B. Leibner, and N. Cohen, "Multistage optical system for broadcasting and switching information," Appl. Opt. **38,** 6103–6110 (1999).
3. D. Marom and D. Mendlovic "All-optical reduced state 4 by 4 switch," Opt. Photon. News (July, 1996), p. 43.
4. T. Stone and J. M. Battiato, "Optical array generation and interconnection using birefringent slabs," Appl. Opt. **33,** 182–190 (1994).